Using Multiple Grids in Markov Mesh Facies Modeling

Heidi Kjønsberg, Marita Stien, Odd Kolbjørnsen, Bjørn Fjellvoll, and Petter Abrahamsen

Abstract We formulate a multi-grid Markov mesh model for geological facies modeling. A hierarchy of nested grids is defined, as well as a Markov mesh model for each grid, but such that it takes into account information also from coarser grids. The result is what we denote a multi-grid Markov mesh model. The framework of generalized linear models and systematic grid specification enable fast parameter estimation. The estimation is done once per grid level. During simulation the coarse patterns are first laid out, and by simulating increasingly finer grids we are able to create patterns at different scales. We apply the method to several tests cases. For each considered training image, the simulation results are quantitatively evaluated by comparing the distribution of the up-scaled permeability tensor of the generated realizations to the permeability tensor of the training image. Also distributions for facies volume fractions are evaluated. We also compare the results of the multi-grid Markov mesh model against the results of a commercially available Snesim algorithm.

Heidi Kjønsberg
Norwegian Computing Center, PO Box 114, Blindern, N-0314 Oslo, Norway, e-mail: Heidi.Kjonsberg@nr.no

Marita Stien
Norwegian Computing Center, PO Box 114, Blindern, N-0314 Oslo, Norway, e-mail: Marita.Stien@nr.no

Odd Kolbjørnsen
Norwegian Computing Center, PO Box 114, Blindern, N-0314 Oslo, Norway, e-mail: Odd Kolbjornsen@nr.no

Bjørn Fjellvoll
Norwegian Computing Center, PO Box 114, Blindern, N-0314 Oslo, Norway, e-mail: Bjorn.Fjellvoll@nr.no

Petter Abrahamsen
Norwegian Computing Center, PO Box 114, Blindern, N-0314 Oslo, Norway, e-mail: Petter.Abrahamsen@nr.no

Ninth International Geostatistics Congress, Oslo, Norway, June 11. – 15., 2012

1 Introduction

The spatial distribution of facies is a crucial part of any reservoir model, since it is often one of the main sources of variability in flow [5]. Multi-point statistics is one class of methods for geological facies modeling, proposed nearly two decades ago [3], and it has developed along two main paths: the statistical model approach [9] and the algorithmic approach [8]. Common to many multi-point methods is the use of a training image that represents the geologic patterns typically found in the reservoir of study. The multi-point methods aim at reproducing the essential aspects of these patterns, but with a variability that can be adapted to the case at hand. When trying to reproduce the patterns, algorithmic multi-point methods tend to produce artifacts in the simulations. This is due to lacking patterns in the training image. Statistical models on the other hand, can interpolate between observed patterns to compute the probability of patterns that are not explicitly present in the training image, and hence artifacts are reduced. With the introduction of Markov mesh models [6], the statistical approach also overcame its original time-consumption problems in parameter estimation and simulation. In this paper we precede yet another step, and formulate a multi-grid Markov mesh model.

The use of multiple grids has previously been used in the algorithmic approach to multi-point methods [7]. The strategy has proved invaluable for capturing patterns at different scales, but without overcoming all the problems of artifacts due to lacking training image patterns. With a multi-grid Markov mesh model we combine an advantage originally developed for algorithmic methods — the use of multiple grids, with the consistency and flexibility of the statistical methods.

Markov mesh models are a sub-class of Markov random fields [9] defined through a unilateral path [2]. In [6] the authors propose to model facies geometries through a single-grid Markov mesh model defined using the framework of generalized linear models [4, 1]. In this paper a hierarchy of grids is defined, and a Markov mesh model analogous to those of [6] is defined for each grid, but such that it takes into account information also from coarser grids. The result is what we denote a multi-grid Markov mesh model. The framework of generalized linear models and systematic grid specification enable fast parameter estimation. The estimation is done once per grid level. During simulation the coarse patterns are first laid out, and by simulating increasingly finer grids we are able to create patterns at different scales.

We present several 3D examples, illustrating that the multi-grid Markov mesh model can be successfully applied for a range of training images. For each considered training image, the simulation results are quantitatively evaluated by comparing the up-scaled permeability tensor of the generated realizations to the permeability tensor of the training image. Also distributions for facies volume fractions are evaluated. The model's ability to reproduce the geological patterns of the training image is evaluated by visual inspection.

2 Multi-grid Markov mesh model

Multi-grid Markov mesh models are defined by a hierarchy of grids, a unilateral path per grid level, and a conditional probability for each cell value given the cell values in a sequential neighborhood. Mathematically, the multi-grid Markov mesh model is nothing but a single-grid Markov mesh model where the cells are visited according to the overall path, and the sequential neighborhood for any cell consists only of cells from the past part of this path. It is nevertheless useful to explicitly discuss the model in terms of the multiple grid levels, since it is systematic model specification in terms of these levels that makes it an efficient and useful tool for capturing patterns at several different scales. For the reader's convenience we start with a small reminder of the single-grid Markov mesh model, then illustrate the idea that multiple grids allows the sequential neighborhood to capture patterns at many different scales, and finally we formulate the multi-grid Markov mesh model itself.

2.1 The single-grid model

Single-grid Markov mesh models are defined by a unilateral path and a conditional probability for each cell value given the cell values in a sequential neighborhood. Consider a finite, regular grid $\mathscr{G}$ in two or more dimensions, and let the one-dimensional index i label the cells of the grid. The set of all cells is $\{1,2,...,N\}$. For the single-grid Markov mesh models this is also the order in which cells are visited during simulation. For each cell i we let the cell value x_i represent the facies of the cell. Assuming that the conditional probability for facies at cell i depends only on a subset Γ_i of all cells $j < i$, we can write this probability as

$$\pi(x_i|x_{j<i}) = \pi(x_i|x_{\Gamma_i}), \tag{1}$$

where x_{Γ_i} is the set of facies values for the cells in the sequential neighborhood. Eq. 1 expresses the Markov property of the model. Figure 1 gives an illustration of a sequential neighborhood on a two dimensional grid. The single-grid Markov mesh

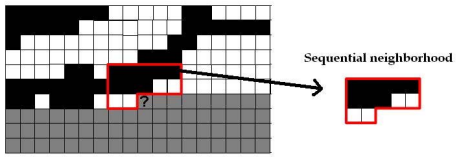

Fig. 1 Illustration of sequential neighborhood. A snapshot of a simulation is displayed, and the grey cells have not yet been simulated.

model is fully specified through the conditional probabilities in Eq. 1, i.e. the joint probability is

$$\pi(x_1, x_2, ..., x_N) = \prod_{i=1}^{N} \pi(x_i | x_{\Gamma_i}). \quad (2)$$

Simulation from the Markov mesh model is performed by following the path $i = 1, 2, ..., N$ throughout the grid. For each cell the facies value is drawn according to the conditional probability $\pi(x_i|x_{\Gamma_i})$. Each cell is visited once, and the resulting grid configuration follows the joint probability distribution in Eq. 2.

2.2 Capturing large scale patterns

The main purpose of using a multi-grid formulation is to be able to detect and reproduce also patterns at a large scale with a relatively small neighborhood. Figure 2 illustrates how this works for a simple 2-dimensional example. The left figure pane shows the sequential neighborhood Γ_i of a reference cell i on the grid $\mathscr{G}$. The right figure pane shows the analogous neighborhood, but applied to the coarser grid level l. The grid $\mathscr{G}_l$ consists of each 2nd and each 4th cell of $\mathscr{G}$, in the horizontal and vertical direction, respectively. Relative to the grids $\mathscr{G}$ and $\mathscr{G}_l$, respectively, the neighborhoods of the left and right figure pane are identical. But measured in terms of cells on the finest grid, i.e. cells on $\mathscr{G}$, the neighborhood reaches much farther when applied to the coarse than to the fine grid. It is this property, that a neighborhood consisting of few cells can reach far in space if applied to a coarse grid, that is used in the multi-grid formulation of the Markov mesh model. It makes it possible to capture patterns even on large scales while retaining a model that is computationally efficient.

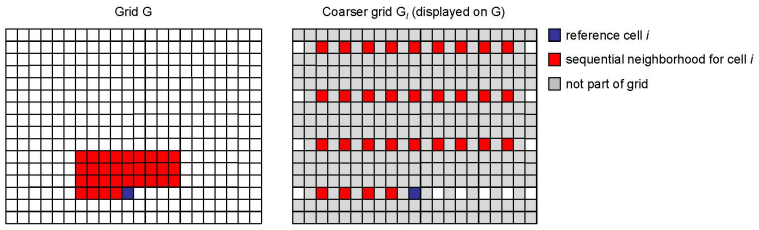

Fig. 2 Left: a sequential neighborhood. Right: the same sequential neighborhood, but on a coarser grid.

2.3 Defining the multi-grid Markov mesh model

We are now ready to present the formulation of the multi-grid Markov mesh model. Consider again a finite, regular grid $\mathscr{G}$ in two or more dimensions, with the one-dimensional index i labelling the cells of the grid. The set of all cells is $\{1,2,...,N\}$. We define a sequence of regular grids $\mathscr{G}_1,\mathscr{G}_2,...,\mathscr{G}_L$, each grid being a subset of $\mathscr{G}$, such that

$$\mathscr{G}_1 \subset \mathscr{G}_2 \subset \mathscr{G}_3 ... \subset \mathscr{G}_L, \text{ and } \mathscr{G}_L = \mathscr{G}. \tag{3}$$

We will refer to $\mathscr{G}_l$ as the grid on level l, with the coarsest grid level being for $l = 1$ and the finest for $l = L$. Define furthermore the disjoint sets $\mathscr{H}_1,\mathscr{H}_2,...,\mathscr{H}_L$ by

$$\mathscr{H}_1 = \mathscr{G}_1, \text{ and } \mathscr{H}_l = \mathscr{G}_l \setminus \mathscr{G}_{l-1}, l = 2,3,...,L. \tag{4}$$

The set $\mathscr{H}_l$ consists of the cells of $\mathscr{G}_l$ that are not on any of the coarser grid levels. Figure 3 gives an example of how a 2-dimensional grid $\mathscr{G}$ can be described in terms of five grid levels.

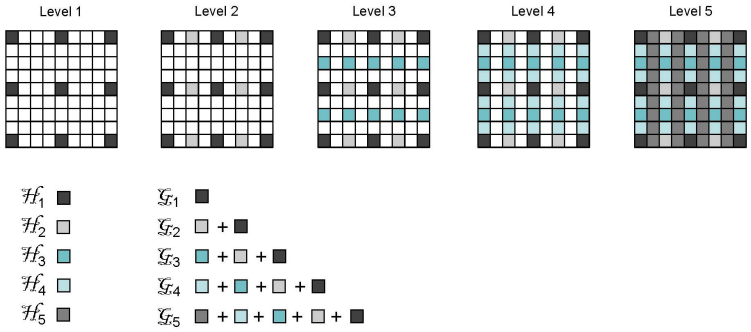

Fig. 3 A hierarchy of grids, displayed as subsets of the set of cells of the finest grid $\mathscr{G}$.

For each set $\mathscr{H}_l$ let $s(l)$ denote the number of cells in $\mathscr{H}_l$, and let p_l be the ordered version of the set of cells on $\mathscr{H}_l$:

$$\begin{aligned} p_l = (i_1, i_2, ..., i_{s(l)}), \quad & \text{where} \\ i_1, i_2, ..., i_{s(l)} \in \mathscr{H}_l, \quad & \text{and} \\ i_q < i_r \text{ if } q < r. & \end{aligned} \tag{5}$$

Here $i_q, \forall q \in \{1,2,...,s(l)\}$ is the original one-dimensional cell index. The last condition says the cells on $\mathscr{H}_l$ are ordered with increasing 1D-index. But be aware that p_l consists only of cells that are on $\mathscr{H}_l$. The ordered set p_l is the unilateral path for grid level l. The total path of the multi-grid Markov-mesh model is defined to be the concatenation of the level-wise paths:

$$p = (p_1, p_2, ..., p_L). \tag{6}$$

The right hand side of Figure 4 shows the order of visiting the cells in a 2D grid, given that the 1D cell indices are as shown in the left-most figure pane, and the grid sequence is as in the example of Figure 3. For given one-dimensional indices, a different grid sequence would imply a different total path.

1	2	3	4	5	6	7	8	9
10	11	12	13	14	15	16	17	18
19	20	21	22	23	24	25	26	27
28	29	30	31	32	33	34	35	36
37	38	39	40	41	42	43	44	45
46	47	48	49	50	51	52	53	54
55	56	57	58	59	60	61	62	63
64	65	66	67	68	69	70	71	72
73	74	75	76	77	78	79	80	81

1	46	10	47	2	48	11	49	3
26	50	27	51	28	52	29	53	30
16	54	17	55	18	56	19	57	20
31	58	32	59	33	60	34	61	35
4	62	12	63	5	64	13	65	6
36	66	37	67	38	68	39	69	40
21	70	22	71	23	72	24	73	25
41	74	42	75	43	76	44	77	45
7	78	14	79	8	80	15	81	9

Fig. 4 Left: One-dimensional cell index. Right: Path order of cells, given the grid sequence of Figure 3.

Since the sets $\mathscr{H}_l$ are disjoint and their union equals $\mathscr{G}$, for each grid cell i, there exists a unique grid level l such that $i \in \mathscr{H}_l$ and $i \notin \mathscr{H}_k$ if $k \neq l$. We write $l(i)$ for this mapping from cell index to grid level, i.e. $i \in \mathscr{H}_{l(i)}$. Given that we follow the path p, all cells that are listed before cell i are given by the set

$$\mathscr{W}_i = \{k | k \in \mathscr{G}_{l(i)-1} \cup \mathscr{P}_i\}_{k=1}^{N}, \tag{7}$$

where

$$\mathscr{P}_i = \{j | j \in \mathscr{H}_{l(i)}, j < i\}_{j=1}^{N}. \tag{8}$$

That is, any cell listed before cell i either belongs to a coarser grid, or is listed before cell i in the unilateral path $p_{l(i)}$ for the grid level associated with i.

For each cell i we let the cell value x_i represent the facies of the cell. The joint probability distribution can always be written as

$$\pi(x_1, x_2, ..., x_N) = \prod_{l=1}^{L} \prod_{i \in p_l} \pi(x_i | x_{\mathscr{W}_i}), \tag{9}$$

since this only amounts to a reordering of the grid cells on the left hand side of the expression, followed by repeated use of the general relation $\pi(A,B) = \pi(A|B)\pi(B)$. Eq. 9 shows how the joint probability distribution of all cells can be expressed in terms of a systematic grid refinement, where the conditional probability $\pi(x_i | x_{\mathscr{W}_i})$ depends only on cells from the present or coarser grid levels, never on cells from finer grid levels.

Now we introduce the Markov condition: we assume that the conditional probability for facies at cell i depends only on a certain subset of the cells from earlier in the path, i.e. we assume that there exists a $\Gamma_i \subset \mathscr{W}_i$ such that

$$\pi(x_i|x_{\mathscr{W}_i}) = \pi(x_i|x_{\Gamma_i}). \tag{10}$$

Then the joint probability can be written

$$\pi(x_1, x_2, ..., x_N) = \prod_{l=1}^{L} \prod_{i \in p_l} \pi(x_i|x_{\Gamma_i}). \tag{11}$$

The set Γ_i is denoted the sequential neighborhood of cell i. It consists of cells from the coarser grids and cells that are listed before cell i on the path p_l. Eq. 11 is a multi-grid Markov mesh model. It is fully specified by the sequence of grid levels and the conditional probabilities $\pi(x_i|x_{\Gamma_i})$. Simulation from the model is carried out by starting at the coarsest grid level, then using increasingly finer grids. At each grid level the unilateral path p_l is followed, and for each cell the facies value is drawn according to the conditional probability $\pi(x_i|x_{\Gamma_i})$. Each cell is visited once, and the resulting grid configuration follows the joint probability distribution in Eq. 11.

3 Model specification

The statistical model is defined by specifying the path and parameterizing the conditional probabilities in Eq. 10. The path is uniquely determined by the sequence of grids. The statistical model specification is based on generalized linear models (GLMs) [4]. Our model specification aims at ensuring efficient parameter estimation and providing good simulation results for a range of training images.

3.1 Specifying the sequential neighborhood

The multi-grid sequential neighborhood is a generalization of the sequential neighborhood of the single-grid Markov mesh formulation, the latter being illustrated on the left hand side of Figure 2. The generalization consists of including in the neighborhood cells with a higher 1D-index, provided they belong to the past path of the reference cell. We illustrate this with an example in Figure 5, where the 1D-indices and path of Figure 4 are reused. The figure gives an example of the sequential neighborhood Γ_{42}. In the example the sequential neighborhood has a maximal extension of two cells in each direction from the reference cell. Now, cell 42 is ordered as number 64 in the path, as indicated in the right hand figure pane. The sequential neighborhood includes only cells with a lower path order number, but as shown by

the left hand figure pane, some of the cells have a 1D-index larger than 42: cells 43, 50, 52, 59, and 61 in this example.

Our specification of the sequential neighborhood consists of, for each grid level specifying its maximal extension in different directions, and then include all cells inside these limits provided they belong to the past path. Since each grid $\mathscr{G}$ is a regular grid, assuming the 1D-indexing is also regular, all cells $i \in \mathscr{H}_l$ are then assigned sequential neighborhoods of exactly the same shape. This is important for the efficiency of the model. For a sequential neighborhood bounded by a rectangular box, six parameters are sufficient for parametrization; if the box is assumed symmetric around the reference cell, three parameters n_x, n_y, n_z suffice. The parameters then typically describe the maximum number of cells in either direction of the reference cell.

1	2	3	4	5	6	7	8	9
10	11	12	13	14	15	16	17	18
19	20	21	22	23	24	25	26	27
28	29	30	31	32	33	34	35	36
37	38	39	40	41	42	43	44	45
46	47	48	49	50	51	52	53	54
55	56	57	58	59	60	61	62	63
64	65	66	67	68	69	70	71	72
73	74	75	76	77	78	79	80	81

1	46	10	47	2	48	11	49	3
26	50	27	51	28	52	29	53	30
16	54	17	55	18	56	19	57	20
31	58	32	59	33	60	34	61	35
4	62	12	63	5	64	13	65	6
36	66	37	67	38	68	39	69	40
21	70	22	71	23	72	24	73	25
41	74	42	75	43	76	44	77	45
7	78	14	79	8	80	15	81	9

Fig. 5 Example of sequential neighborhood Γ_{42}. Left pane: 1D cell indices; Right pane: order of cells in the path.

Figure 6 illustrates a symmetrically bounded sequential neighborhood in 3D by displaying four z-layers for a given grid $\mathscr{G}_l$. Only cells on grid $\mathscr{G}_l$ are shown, not for any finer grid levels. It is assumed that $n_x = n_y = 3$ and $n_z = 2$, and that the 1D cell index loops first over the x-direction, then the y-direction, and last the z-direction. Three different cases are shown: In Case 1 it is assumed that grid $\mathscr{G}_l$ is related to the coarser grid $\mathscr{G}_{l-1}$ by a refinement in the z-direction. By this we mean that if grid $\mathscr{G}_{l-1}$ consists of each 2^{k_x}, 2^{k_y}, 2^{k_z} cells of the finest grid $\mathscr{G}$, then $\mathscr{G}_l$ consists of each 2^{k_x}, 2^{k_y}, 2^{k_z-1} cells. In Case 2 the refinement was done in the y-direction, and in Case 3 the refinement was done in the x-direction. The figure illustrates how the sequential neighborhood depends on the grid sequence.

3.2 Using the framework of generalized linear models

The use of GLMs for specifying Markov mesh models for facies modeling was first suggested in [6]. The idea in GLM is that the distribution of a response variable

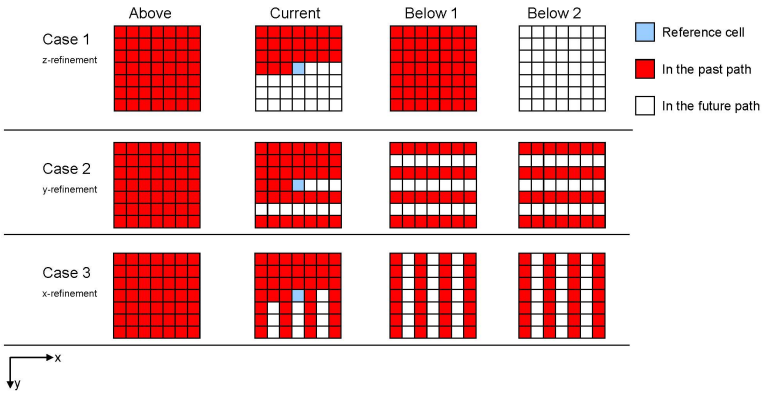

Fig. 6 The sequential neighborhood for each of three grid refinement cases, provided the neighborhood's maximal extension is $n_x = n_y = 3$ and $n_z = 2$. The sequential neighborhood consists of the cells in the past path.

depends on a linear combination of explanatory variables through a non-linear link function. We let the facies x_i be the response variable, and the explanatory variables be functions of the sequential neighborhood Γ_i.

Consider a given grid level l and let the cell i be on this grid level, i.e. $i \in \mathscr{H}_l$. Let $\mathbf{z}_i$ be a P_l-dimensional vector of explanatory variables with elements that are functions of cells from the sequential neighborhood Γ_i. We propose particular functions below, but for now simply write $z_{ij} = f_j(x_{\Gamma_i})$ for $j \in \{1,2,...,P_l\}$. The same set of P_l functions is used for any neighborhood Γ_i if $i \in \mathscr{H}_l$. The value $f_j(x_{\Gamma_i})$ varies with i, since it depends on the facies configuration in the neighborhood Γ_i. For each grid level l there is one model parameter per neighborhood function per facies value. Assuming there are K different facies values, we let the K vectors $\theta_l^1,...,\theta_l^K$ hold the parameters. Each vector is P_l-dimensional.

We encode the cell value $x_i \in \{1,2,...,K\}$ with binary variables x_i^k such that

$$x_i^k = \begin{cases} 1 & \text{if } x_i = k\,, \\ 0 & \text{otherwise.} \end{cases} \tag{12}$$

The conditional probability in Eq. 10 is then

$$\pi(x_i|\Gamma_i) = \pi(x_i|\mathbf{z}_i, \theta_{l(i)}^1,...,\theta_{l(i)}^K) = \frac{\prod_{k_1=1}^K \exp\left\{x_i^{k_1}\mathbf{z}_i^T\theta_{l(i)}^{k_1}\right\}}{\sum_{k_2=1}^K \exp\{\mathbf{z}_i^T\theta_{l(i)}^{k_2}\}}, \tag{13}$$

and the joint probability in Eq. 11 is

$$\pi(x_1,x_2,...,x_N) = \prod_{l=1}^{L}\prod_{i\in p_l} \frac{\prod_{k_1=1}^{K} \exp\left\{x_i^{k_1}\mathbf{z}_i^T\theta_l^{k_1}\right\}}{\sum_{k_2=1}^{K}\exp\{\mathbf{z}_i^T\theta_l^{k_2}\}}. \quad (14)$$

Here p_l is the path on grid level l. Interpreted as a likelihood for the model parameters Eq. 14 is a GLM for each grid level. The maximum likelihood estimation of the parameters in the multi-grid Markov mesh formulation can therefore be solved with the iterative weighted least squares scheme. Parameter estimation is for a single-grid Markov mesh model discussed in [6], and their methods can be directly applied to each grid level of our multi-grid approach.

3.3 Neighborhood functions

As noticed by [6], the challenge with multi-point statistics is that there generally are too many possible patterns. A finite training image does not hold information about all possibilities, and computationally it is impossible to handle them all anyway. To come around this problem we extract a subset of properties, represented by the neighborhood functions, that we believe are important in order to reproduce geological structures. We do not expect our subset to be suited for all possible training images, but nevertheless aim at making robust choices. It is possible to achieve other characteristics by adding or removing neighborhood functions, while retaining the GLM formulation of a multi-grid Markov mesh model.

Our specification of the neighborhood functions is similar to the specification of [6] in the sense that the 3D model consists of combining three 2D models, one for each of three orthogonal grid slices intersecting at the reference cell, adding a few off-2D extensions; and we focus on two point interactions, multi-point interactions representing continuity and transitions of facies, and multi-point interactions representing all possible patterns for a very limited number of cells.

It differs from the specification of [6] in the sense that we take into account also functions for cells with a higher 1D index than the reference cell, provided they are part of the multi-grid sequential neighborhood.

3.3.1 Two-dimensional specification

For each 2D grid slice of the sequential neighborhood of the reference cell i, the 2D two-point interactions are restricted to a subset of the slice in question. For each cell j of this subset, indicator functions $f^k(x_j)$ are included, one for each facies $k \in \{1,2,...,K\}$. The functions are defined by

$$f^k(x_j) = \begin{cases} 1 & \text{if } x_j = k\,, \\ 0 & \text{otherwise.} \end{cases} \quad (15)$$

This gives one function per facies per two-point interaction cell, with one model parameter per function.

For each 2D grid slice, the multi-point functions representing connectivity and transition of facies are also represented by indicator functions. Each function is defined relative to a certain set of cells. Let γ_i^{l-1} be a set of $l-1$ neighbors of the reference cell i, corresponding to an l-point interaction term [6]. The indicator function $f^k(x_{\gamma_i^{l-1}})$ is then defined by

$$f^k(x_{\gamma_i^{l-1}}) = \begin{cases} 1 & \text{if } x_j = k, \forall j \in \gamma_i^{l-1}, \\ 0 & \text{otherwise.} \end{cases} \tag{16}$$

The sets γ_i^{l-1} are defined by considering strips of cells in the horizontal, vertical and diagonal directions of the 2D slice. See [6] for a more detailed presentation on this. Input parameters can be used to define the maximal length of the strips, and how many strips to use. More and longer strips imply more indicator functions, and hence more model parameters.

Indicator functions are also used for the multi-point interactions representing all possible patterns for a very limited number of cells in the 2D grid slice. There is one function per facies per pattern of the neighboring cells, resulting in K^n functions if $n-1$ neighbors participate to this kind of multi-point interaction.

3.3.2 Three-dimensional specification

The 3D model is defined by using the combined set of indicator functions from the three 2D grid slices. We also include strips in the off-2D diagonal directions of each of the eight octants centered around the reference cell i, using only the octant cells that are part of the multi-grid sequential neighborhood. This is analogous to the specification of [6]. The resulting number of functions for the 3D model is denoted P_l, where l labels the grid level.

The set of neighborhood functions generally differs across the grid levels, but for a given level l the same set of P_l functions is used for all cells $i \in \mathscr{H}_l$. Figure 7 illustrates some of the 2D neighborhood functions for the case of a grid $\mathscr{G}_l$ that is assumed related to grid $\mathscr{G}_{l-1}$ by a refinement in the y-direction (second row of Figure 6). Only the z-plane of the reference cell is shown in Figure 7. The left column of the figure illustrates functions that would have been used if the sequential neighborhood were identical to its symmetrical bounding box; the rightmost column illustrates what the actual neighborhood functions look like after the form of the sequential neighborhood for this grid level is taken into account; and the middle column illustrates the filtering that takes us from the general functions of the left column to the grid level specific functions of the right.

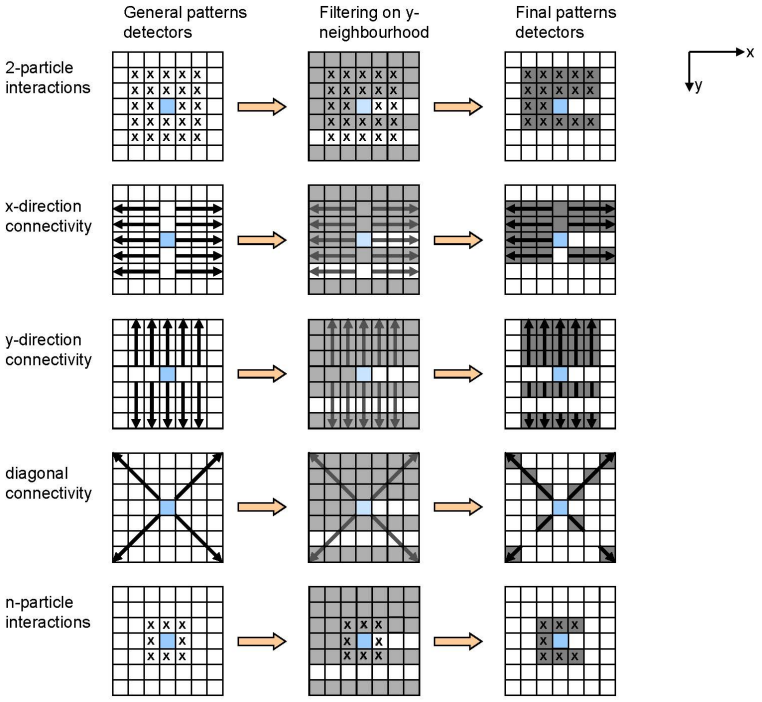

Fig. 7 A 2D example of how general pattern recognition functions are modified by the sequential neighborhood to form the grid specific neighborhood functions. The arrows indicate the directions and in which order the number of interaction terms increases.

3.4 Grid refinement

The model of Eq. 14 is partly specified by the choice of explanatory variables (neighborhood functions), partly by the choice of the multi-grid path. In our formulation the path is uniquely determined by the choice of multi-grid sequence, given the 1D indices for the grid cells. For a given training image, two different grid sequences will represent two models, and hence give different simulation results. No single grid sequence works equally well for all training images.

For determining the coarsest grid $\mathscr{G}_1$ we suggest using the idea that when using a coarse grid, it is possible to capture large scale patterns even if the neighborhood consists of a rather limited number of cells (Figure 2). Our solution consists of estimating the TI's correlation ranges, then choosing the coarsest grid such that a user specified neighborhood, when applied to this grid, reaches just beyond the maximal correlation ranges in each direction.

For the subsequent grid sequence, our best results have been achieved when refining the grid in one direction at the time. That is, any grid $\mathscr{G}_l$ is related to the previous level's grid, $\mathscr{G}_{l-1}$ by a refinement of the x–, y–, or z-direction, but never

by a combination of the three. We suggest to use the estimated TI correlations also for determining this grid sequence, thus tailor-making the sequence to the training image in question. By using the refinement direction for which the estimated correlations are weakest, the simulation algorithm is given maximal freedom to lay out a variety of patterns at each grid level. This ensures statistical variability in the simulation results.

4 Examples

This section presents results obtained by using the multi-grid Markov mesh model. We consider four different 3D training images, three with two facies classes, one with three facies classes. For each training image we study the conceptual geology, the effective permeability, and the facies volume fractions. We provide a comparison between the results of the multi-grid Markov mesh model and the algorithmically driven, multi-grid, Snesim approach ([8], [7]). The latter is obtained through running the multipoint module of a commercial software.

For each training image we have simulated 100 realizations with the multi-grid Markov mesh model, and 100 realizations with the Snesim algorithm. Each realization was subsequently run through an algorithm that computes the effective permeability of the realization volume. The effective permeability is calculated also for the training image. The statistical distribution for the realizations' effective permeability tensor can then be compared directly to the effective permeability of the training image. For each realization we also compute the facies volume fractions, and compare the statistical distributions to the volume fractions of the training image. Statistical distributions for effective permeability and volume fractions is obtained separately for the multi-grid Markov mesh model and for the Snesim approach, one distribution per training image. Each distribution is based on 100 realizations.

Conceptual geology is assessed by visual inspection. We here present the results of one simulated multi-grid Markov mesh realization and one Snesim realization per training image. For each training image the shown realization is representative for the set obtained.

4.1 Conceptual geology

For each of four different training images, Figures 8, 9, 10, and 11 compare the conceptual geology of a multi-grid Markov mesh realizations and a Snesim realizations to the training image. Each of the four figures show the training image to the left, a realization obtained by the multi-grid Markov mesh model in the middle, and a realization obtained by the Snesim algorithm to the right. The training images represent, respectively, a turbidite system (Figure 8); a channels system where the main correlations are not along the main axis of the simulation box, but rather along the

x, y-diagonal, and where the channels are somewhat narrow and irregular (Figure 9); a system of irregular channels with crevasses (Figure 10); and a system of regular channels with fairly low sinuosity (Figure 11).

The simulated realizations clearly illustrate that the multi-grid Markov mesh model easily reproduces main aspects of the training image, such as correlation directions and body shapes. There is in general no major difference between the visual appearance of the multi-grid Markov mesh realizations (middle) and the realizations obtained by the multi-grid Snesim approach (right).

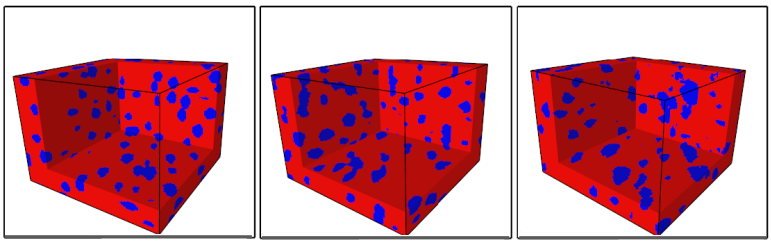

Fig. 8 Conceptual geology, turbidite case. Training image: left, multi-grid Markov mesh model: middle, Snesim algorithm: right.

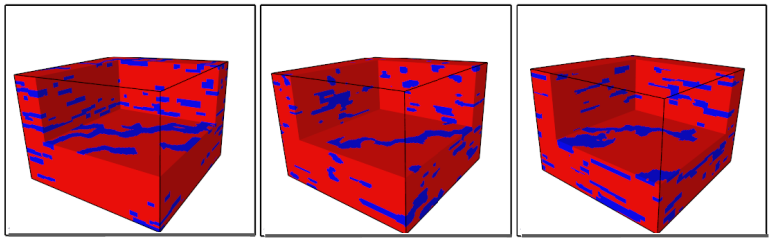

Fig. 9 Conceptual geology, azimuth channels case. Training image: left, multi-grid Markov mesh model: middle, Snesim algorithm: right.

4.2 Effective permeability

Figures 12 and 13 display the effective permeability tensors for the whole volume of the realizations and training image. The tensors are in general symmetric, 3-dimensional tensors of second order. We include here only the diagonal elements, representing permeability in the xx-, yy-, and zz-direction. With respect to evaluating the multi-grid Markov mesh model to the training image and the Snesim algorithm,

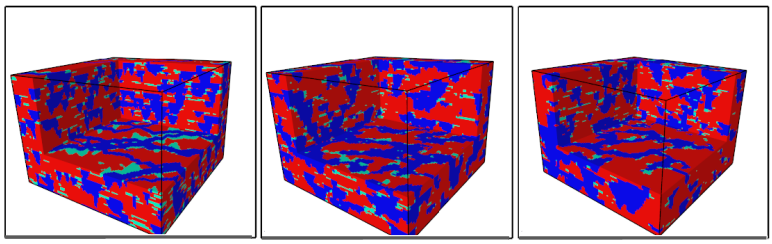

Fig. 10 Conceptual geology, channel crevasse case. Training image: left, multi-grid Markov mesh model: middle, Snesim algorithm: right.

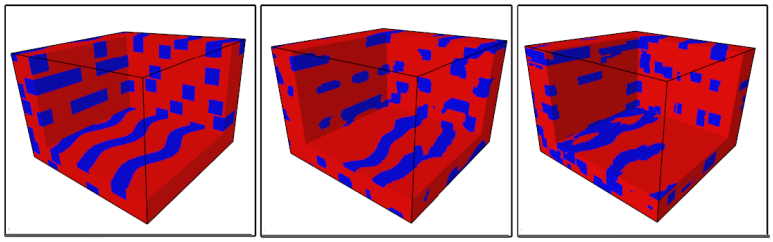

Fig. 11 Conceptual geology, isolated channels case. Training image: left, multi-grid Markov mesh model: middle, Snesim algorithm: right.

the results of the off-diagonal elements provide no further insight, and are hence omitted here. For each training image, the results for the multi-grid Markov mesh model are displayed in the top row, and the results for the Snesim algorithm are displayed in the bottom row. For each tensor component, the probability distributions obtained from simulations are shown in blue, while the red line indicates the corresponding permeability of the training image.

For the turbidite case (left figure pane, Figure 12) both the multi-grid Markov mesh model and the Snesim algorithm reproduce the training image's permeability tensor very well; the red line is well inside the distributions, often corresponding to the mean of each distribution. There is a small exception for the Snesim approach's zz-permeability, but the percent-wise deviation between the training image permeability and the mean Snesim permeability is tiny. With more statistics (more simulated realizations) the width of the distribution is very likely to include the training image permeability.

For the azimuth channels case, the distributions for the xx- and yy-permeability contain the training image permeability for both the multi-grid Markov mesh model and the Snesim algorithm. But for both methods the training image permeability is in the tail, not so close to the mean, of the distributions. The multi-grid Markov mesh model tends to make realizations with too little connectivity, the Snesim approach tends to make too much connectivity. It is reasonable that the results for the xx-permeability is similar to the results for the yy-permeability, since the training

image in this case has its main correlations along the x,y-diagonal and hence is symmetric for x and y. The minute training image permeability in the zz-direction is under-estimated/over-estimated by the multi-grid Markov mesh model and the Snesim algorithm, respectively. But the percent-wise deviation is very small.

For the channel crevasse case and the isolated channels, both the multi-grid Markov mesh model and the Snesim algorithm capture the scale of the permeabilities, with small percent-wise deviations from the training image permeabilities. For these training images the two methods behave very similar: they both have a tendency to underestimate the xx- and yy-permeabilities for the channel crevasse case and for the yy-permeability of the isolated channels; they both overestimate the xx-permeability of the isolated channels; and they both tend to slightly overestimate the zz-permeabilities.

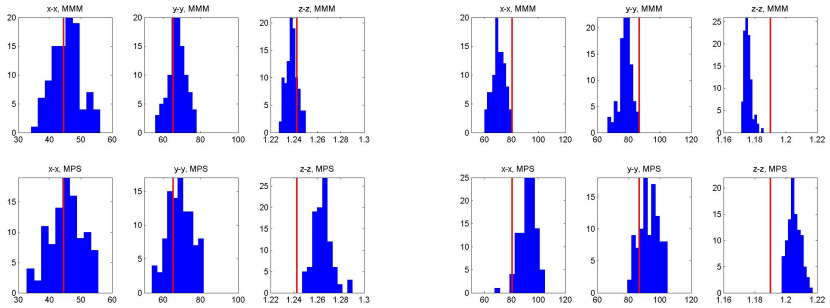

Fig. 12 Effective permeability. Left: turbidite case, right: azimuth channels case. Upper row: multi-grid Markov mesh model; lower row: Snesim algorithm. Red line: training image's effective permeability.

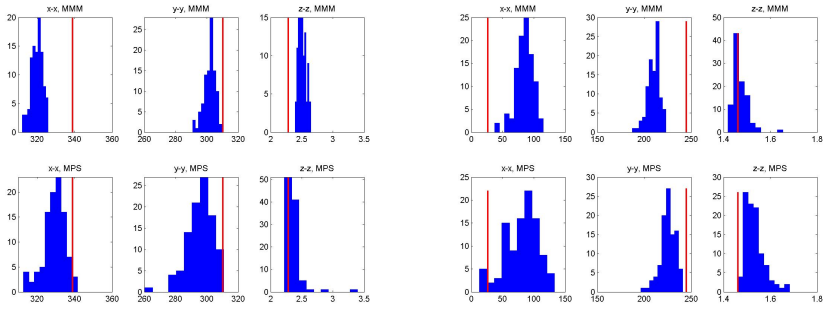

Fig. 13 Effective permeability. Left: channels crevasse case, right: isolated channels case. Upper row: multi-grid Markov mesh model; lower row: Snesim algorithm. Red line: training image's effective permeability.

4.3 Volume fractions

Figures 14 and 15 compare the volume fraction distributions to the training images' volume fractions. For easier comparison across training images the scale of the horizontal axis is the same in all figures. The ability of the multi-grid Markov mesh model in reproducing the training images' volume fractions is comparable to the ability of the Snesim algorithm.

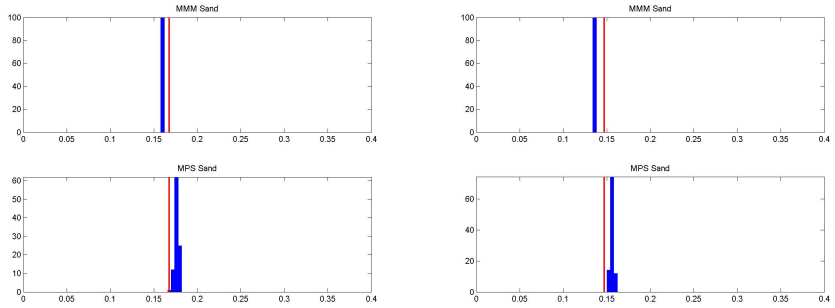

Fig. 14 Volume fractions. Left: Turbidite case, right: azimuth channels case.

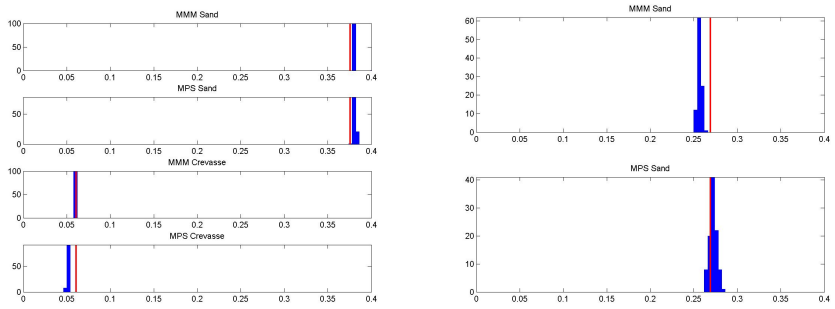

Fig. 15 Volume fractions. Left: Channels crevasse case, right: isolated channels case.

5 Conclusions

We have presented a multi-grid Markov mesh model for geological facies modeling. This combines an advantage originally developed for algorithmic multipoint meth-

ods — the use of multiple grids — with the flexibility and consistency of the statistical approach to multipoint methods. The model consists of a hierarchy of nested grids, with a single-grid Markov mesh model for each grid, but such that information from coarser grids are taken into account. We have adopted the specification of earlier published single-grid Markov mesh models, by using the framework of generalized linear models and a parametrization that captures continuity/discontinuity of geological structures. The result is a model that is efficient and gives results comparable to that of a commercially available software based on the Snesim algorithm. The comparison of results is carried out for four different training images. Reproduction of conceptual geology, efficient permeability, and facies volume fractions were used as comparison criteria.

Acknowledgements We would like to thank Statoil and Roxar for financial support, and for making available the tool for doing permeability upscaling and the Irap RMS software. We would also like to thank the Norwegian Research Council for financial support.

References

1. Cressie, N., Davidson, J.: Image analysis with partially ordered markov models. Computational Statistics and Data Analysis, **2**9(1), 1–26 (1998)
2. Daly, C.: Higher order models using entropy, markov random fields and sequential simulation. In: Leuangthong, O., Deutsch, C. (eds.), Quantitative Geology and Geostatistics, Geostatistics Banff 2004, pp. 215–224. Springer, Dordrecht, The Netherlands (2005)
3. Guardiano, F., Srivastava, R.M.: Multivariate geostatistics: Beyond bivariate moments. In: Soares, A. (ed.), Geostatistics-Troia,**1**, pp. 133–144. Kluwer, Dordrecht (1993)
4. McCullagh, P. and Nelder, J.: Generalized Linear Models. Chapman and Hall, 2. edition. (1989)
5. Skorstad, A., Kolbjørnsen, O., Fjellvoll, B., Howell, J.: Sensitivity of oil production to petrophysical heterogeneities. In: Leuangthong, O., Deutsch, C. (eds.), Quantitative Geology and Geostatistics, Geostatistics Banff 2004, pp. 723–730. Springer, Dordrecht, The Netherlands (2005)
6. Stien, M., Kolbjørnsen, O.: Facies modeling using a Markov mesh model specification. Mathematical Geosciences (2011) doi: 10.1007/s11004-011-9350-9
7. Strebelle, S.: Conditional simulation of complex geological structures using multiple-point statistics. Mathematical Geology, **3**4(1), pp. 1–22 (2002)
8. Strebelle, S., Journel, A.: Sequential simulation drawing structures from training images. In: Kleingeld, W., Krige, D. (eds.), Geostatistics Capetown 2000, **1**, pp. 381–392. (2000)
9. Tjelmeland, H., Besag, J. E.: Markov random fields with higher-order interactions. Scand. J. Statist., **2**5(3), pp. 415–433 (1998)